Femtosecond pump-probe studies of carrier transport and gain dynamics in quantum cascade lasers

Hyunyong Choi[1], Laurent Diehl[2], Marcella Giovannini[3], Jérôme Faist[3], Federico Capasso[2], and Theodore B. Norris[1],*

[1] Center for Ultrafast Optical Science and Department of Electrical Engineering and Computer Science, University of Michigan, Ann Arbor, MI 48109-2099, USA

[2] Institute of Physics, University of Neuchâtel, 2000 Neuchâtel, Switzerland

[3] School of Engineering and Applied Sciences, Harvard University, Cambridge, Massachusetts 02138, USA

* Corresponding author: e-mail tnorris@eecs.umich.edu, Phone: +1-734-7649269, Fax: 1-734-7634876

Time-resolved pump-probe differential transmission measurements have been performed on various sets of quantum cascade lasers below and above threshold. Bias-, temperature-, and polarization dependent studies enable a comprehensive understanding of the gain dynamics to be possible in terms of tunneling, transport, and coupling with the intra-cavity photon density.

1 Introduction In a quantum cascade laser (QCL), electrons are injected into the cascade heterostructures, ideally emitting one photon via stimulated emission in each active region [1]. Thus QC operation results from a coupling of the perpendicular transport of electrons with the intra-cavity optical intensity.

In this work, we investigated the transport of electrons in QCL's below and above threshold by time-resolving the gain dynamics in a femtosecond pump-probe experiment. In the first set of QCL's where the lasing transition is vertical, we observed both fast (< 1 ps) and slow (∼ 2-5 ps) gain recovery components, and interpreted them in terms of resonant tunneling and superlattice transport. In the second set of QCL's where the lasing transition is diagonal in real space [2], studies of the near-threshold revealed that the transport of electrons is driven by the quantum stimulated emission by the intra-cavity photon density.

2 Experimental For the femtosecond time-resolved pump-probe differential transmission (DT) spectroscopy, mid-infrared (IR) pulses were generated from an Optical Parametric Amplifier (OPA) and Difference Frequency Gen-

erator (DFG) pumped by a 2500-kHz, 800-nm Ti:Sapphire regeneratively amplified system. The experimental scheme is shown in Fig. 1. The mid-IR pulses were tunable from 2.5 to 7.5 µm, and the typical pulse width was ∼ 250 fs, which determines the temporal resolution of our DT measurements. The femtosecond mid-IR pump and probe pulses were at the same wavelength (degenerate pump-probe), tuned to be resonant with the QCL emission wavelength. The polarizations of the pump and probe beams were oriented at ± 45° with respect to the transverse magnetic (TM) lasing mode of the QCL. In this configuration, the scattered or transmitted pump beam was isolated before the probe beam detection by a polarizing analyzer, and a 10-µm spatial filter was carefully positioned before the probe beam detection in order to isolate the portion of the probe coupled into the waveguide.

3 Results and discussion

3.1 Vertical transition QCL A schematic of band structure for the first set of QCL samples is shown in Fig. 2. Details of the QCL sample used in this experiment are given in Ref. [3]. In Fig. 3(a), we show series of gain recov-
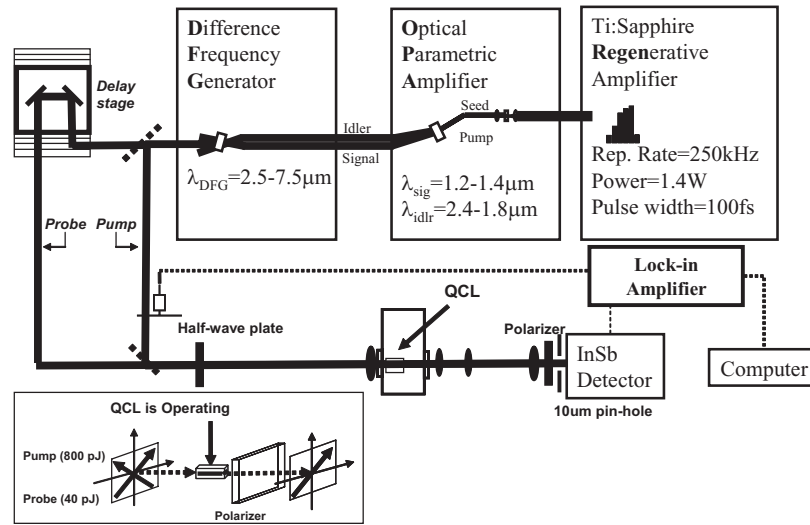
Figure 1 Experimental setup for the time-resolved degenerate pump and probe experiment.
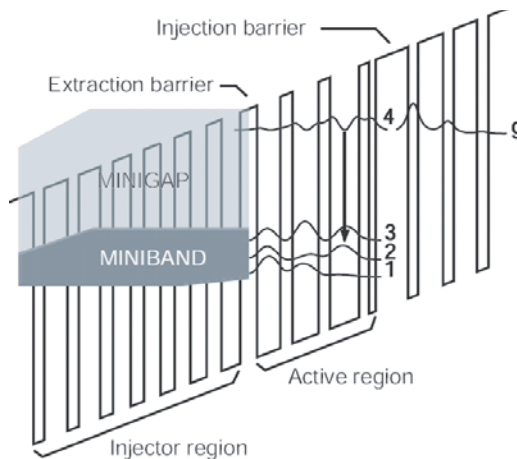

Figure 2 Bandstructure diagram for the first set of QCLs. An electric field of 68 kV/cm was applied to align the structure. The $In_{0.61}Ga_{0.39}As/In_{0.45}Al_{0.55}As$ layer sequence of one period of the active region, starting from the injection barrier is as follows: **46**/9/**14**/41/**16**/37/**17**/33/**24**/26/**21**/23/**22**/20/**23**/19/bf25/18/**30**/16/**33**/15/**35**/14. Thicknesses are in Angstrom, barrier layers are in bold, quantum-well layers are in roman, doped layers (Si, 2.65×10^{11} cm^{-2}) are underlined. The lasing wavelength was 4.58 μm with the threshold current ranging from 171 mA at 10 K to 279 mA at 100 K.

Figure 3 (a) Pump-probe transient signals measured at various bias currents at 78 K. Carrier heating by TE-pump and TM-probe measurement is shown on the top of the gain recovery signal. (b) Normalized and fitted DT signal at 275 mA bias current.

ery DT signals at various bias currents at 78 K; in Fig. 3(b), one of the normalized curves at 275 mA including the rate-equation fit is displayed.

Depletion of the gain induced by the pump gives rise to a negative probe DT signal near zero time delay because of the strong stimulated emission. Independent TE-pump and TM-probe DT measurements were performed in order to isolate carrier heating effects. Since optical inter-
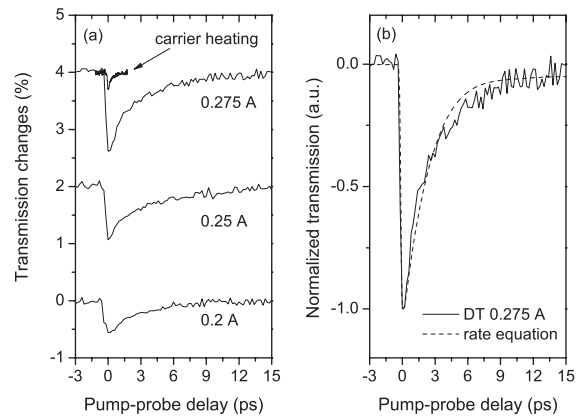
subband transitions only occur for the TM polarized beam (z-growth direction), the non-resonant TE-polarized pump excites the electrons into the continuum state and generates hot carriers. As shown in Fig. 3(a), carrier heating contributions were experimentally shown to be negligible.

Figure 4(a) shows the two exponential time constants from fits of the DT data as a function of bias current. A "fast" component (< 1 ps) of the initial gain recovery was observed at all bias and temperature conditions investigated; this is attributed to a carrier refilling process from the injector ground state into the upper lasing state in the active region via resonant tunneling. No coherent tunneling oscillations were observed under any bias conditions. This indicates that coherent tunneling oscillations are strongly damped by dephasing collisions in the coupled states [4].
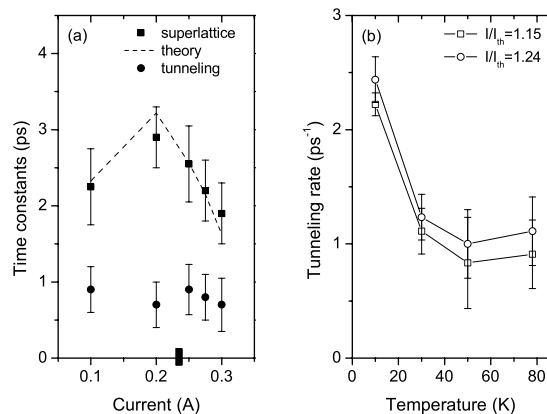
Figure 4 (a) Gain recovery time constants for each bias current. Filled circles represent the fast component and filled square are the slow component. Threshold current is indicated as a black tick mark. (b) Temperature dependent fast recovery components at two different bias currents.

Strong dephasing comes from the extremely fast electron-electron scattering (< 100 fs) and the onset of plasmon emission in the upper lasing subband. As can be seen in Fig. 4(b), the resonant tunneling rate was found to decrease with increasing temperature over the temperature range investigated from 10 K to 78 K. This is consistent with the resonant tunneling model of Eq. (1) [1] and Ref. [4], where it is shown that the resonant tunneling rate decreases with increasing dephasing of the tunnel-coupled states. The tunneling rate is

$$\frac{1}{\tau_1} = \frac{\Omega_R{}^2 \frac{1}{2}\left(\frac{1}{\tau_\perp}\right)}{\left(\frac{1}{\tau_\perp}\right)^2 + \left(\frac{\Delta E}{\hbar}\right)^2} \qquad (1)$$

where $1/\tau_1$ is the temperature dependent tunneling rate, $\hbar\Omega_R$ is the energy splitting between injector ground state and upper lasing state in the active region, $1/\tau_\perp$ is the dephasing rate, and ΔE is the energy detuning between injector ground state and upper lasing state in the active region in the absence of coupling.

We also observed a "slow" recovery component with a time constant of 2-5 ps at all bias currents and temperature ranges. The slow component is due to electron transport through the superlattice miniband in the injector region [6]. This component shows a characteristic bias dependence. When electrons tunnel from the lower lasing state into the superlattice following pump-pulse-induced stimulated transitions, a perturbation is induced on the equilibrium electron density profile in the superlattice. The equilibrium carrier density profile is restored in the superlattice in a manner analogous to the dielectric relaxation. We

---

[1] This equation can be derived from the two-level density matrix theory [5], and is found to be exactly same as Eq. (4) in Ref. [4]: the tunneling rate is inversely proportional to the dephasing collision rate in the upper lasing state.
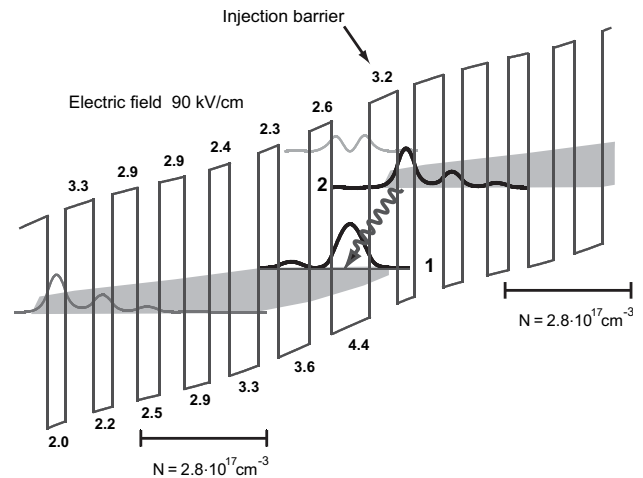

Figure 5 Self-consistent band structure calculation of the In$_{0.6}$Ga$_{0.4}$As/In$_{0.44}$Al$_{0.56}$As strained layers for two periods of the cascade heterostructure (N-432). Layer thicknesses are given in nm. The wavefunctions for the upper (level 2) and lower lasing state (level 1) are shown, illustrating the diagonal nature of the transition in real space. The wavy arrow indicates the lasing transition. The miniband is indicated by the shaded gray region. The horizontal segments show the doped region for each period; N is the donor density. Another QCL sample used in this experiment (N-433) with slightly different design parameters shows similar laser performance.

developed an ensemble Monte-Carlo simulation [7] taking into account the inhomogeneous electric-field distribution in the superlattice at each bias condition. The result is shown as a dashed line in Fig. 4, showing good agreement between the experimental data and the dielectric relaxation model.

3.2 Superdiagonal QCL The second set of QCL's used in this experiment is shown in Fig. 5 and is based on a 'diagonal transition' where the lasing transition is controlled by tuning the oscillator strength through the linear Stark effect [2]. Two QCL's (N-432 and N-433) processed with different cavity length and width were studied. The lasers operated in continuous-wave mode during the experiments. The emission wavelength near threshold and the pump-probe wavelengths were around 5.2 μm. In this structure, there is no resonant tunneling injection process to achieve the population inversion, and thus the superlattice transport directly connects the adjacent active regions.

The main result of this report is contained in Fig. 6, showing the upper state lifetime τ_2, obtained from the rate-equation fits of the DT as a function of bias current. Well below threshold τ_2 is determined by the phonon-assisted relaxation to the lower state. As the bias approaches threshold from below, quantum stimulated emission begins to drive the diagonal lasing transition. Since the current through any level in the QC structure is $J = qn_j/\tau_j$, where n_j is
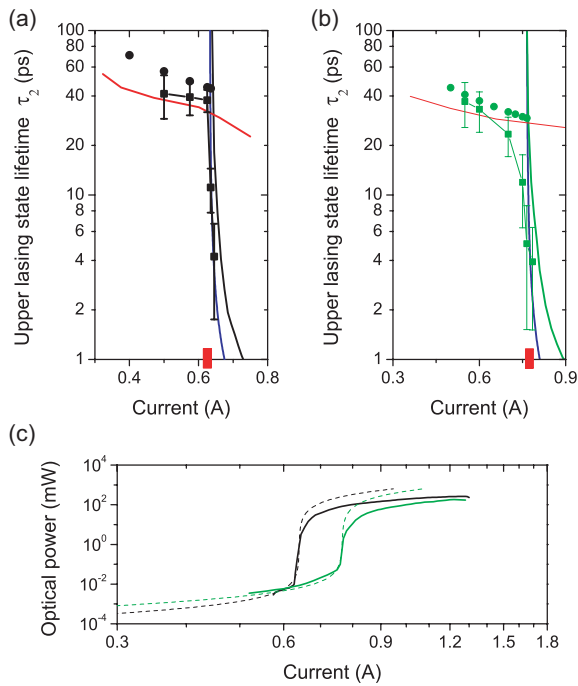
Figure 6 Bias-dependent level-2 lifetime τ_2 is shown for N-432 in (a) and N-433 in (b) (threshold is indicated by the red tick mark). The filled squares are the level-2 lifetime obtained from rate-equation fits to the gain recovery DT data. The horizontal red solid lines in (a) and (b) are the level-2 lifetime due to optical-phonon scattering calculated using the bias-dependent wavefunctions; the errors obtained by assuming monolayer fluctuations of the barrier width are around 10 ps, which is within our measurement. The filled circles are an estimate of the level-2 lifetime using $J = qN/\tau_2$ and assuming the level-2 population N is simply the doping density. The dramatic reduction in lifetime just below threshold corresponds to the onset of stimulated emission. The stimulated emission lifetime τ_{st} was obtained in two ways, using the L-I curves shown in (c). First, τ_{st} was calculated directly by obtaining the cavity photon density S from the measured output power (solid line in (c)) and using $\tau_{st} = N/v_g N_p g_c S$, where N is the population inversion (again assumed to be the doping density), v_g is the group velocity, N_p is the number of cascading stages (=25 in our QCL), and g_c is the gain cross-section; the result is shown as the black and green solid vertical line in (a) and (b), respectively. Secondly, the rate-equation model was used to fit the L-I curves (dashed line in (c)), and the resulting values of S were used to calculate τ_{st}. The result is the blue solid vertical line in (a) and (b). The only free parameter required to fit the L-I curves with the rate-equation model is the β factor.

the density in level j and τ_j is the state lifetime, we see that as the stimulated emission turns on, the current through the QC structure is driven by the photon emission, and τ_2 becomes the stimulated emission lifetime.

The strong variation of the upper state lifetime in the vicinity of the threshold appearing in the gain recovery is due to two factors unique to QCL's. First, unlike traditional lasers, the gain recovery is not determined just by the upper state lifetime but also by a transport delay through the superlattice which is of the same order of magnitude. Secondly, below threshold the upper state lifetime is almost entirely non-radiative. Due to the large spontaneous emission factor of 10^{-3} measured for these lasers, the stimulated emission rate speeds up rapidly just below threshold; application of the rate equation model to the steady-state L-I characteristics shows that the stimulated lifetime becomes of the order of the non-radiative lifetime (40 ps) with only of the order of 100 photons in the cavity.

4 Conclusion In conclusion, we report time-resolved gain recovery dynamics of resonant tunneling, superlattice transport, and photon-driven transport in operating QCL's. The observed transient negative DT signals are due to the strong stimulated emission from the upper lasing state to the lower lasing state. Through polarization dependent DT measurements, gain compression due to carrier heating is experimentally shown to be small compared to the stimulated emission. Bias- and temperature-dependent recovery dynamics show that the resonant tunneling is incoherent due to the strong dephasing collisions in the active sub-band. On a longer time scale (few-ps) the gain recovers to its steady-state value via dielectric relaxation in the superlattice. For the QCL's with the diagonal transition, we observed for the first time how the transport of electrons is driven by the quantum stimulated emission as the bias approaches the threshold.

References

[1] J. Faist, F. Capasso, D. L. Svico, C. Sirtori, A. L. Hutchinson, and A. Y. Cho, Science **264**, 553-556 (1994).
[2] J. Faist, F. Capasso, C. Sirtori, D. L. Svico, A. L. Hutchinson, and A. Y. Cho, Nature **387**, 3477-3479 (1997).
[3] J. Faist, D. Hofstetter, M. Beck, T. Aellen, M. Rochat, and S. Blaser., IEEE J. Quantum Electron. **38**, 533-546 (2002).
[4] K. Leo, J. Shah, J. P. Gordon, T. C. Damen, D. A. B. Miller, C. W. Tu, and J. E. Cunningham, Phys. Rev. B **42**, 7065-7068 (1990).
[5] P. W. Milonni and J. H. Eberly, Lasers (John Wiley & Sons, New York, 1988); A. Yariv, Quantum Electronics, 3rd ed. (John Wiley & Sons, New York, 1989).
[6] B. Deveaud, J. Shah, and T. C. Damen, B. Lambert, and A. Regreny, Phys. Rev. Lett. **58**, 2582-2585 (1987).
[7] Z.-J. Wu , H. Choi, X. Su, S. Chakrabarti, P. Bhattacharya, and T. B. Norris, IEEE J. Quantum Electron. **43**, 486-496 (2007).